Journal of Marine Biology & Oceanography

Research Article

Impact of Tropical Cyclones on Physical and Biological Response of the Bay of Bengal Using Observations and Model Simulations

Suchita Pandey[1]*, Chirantan Bhagawati[2], Pavan Harika Raavi[3] and Arun Chakraborty[4]

[1]Department of Atmospheric and Ocean Studies, University of Allahabad, Uttar Pradesh, India

[2]Department of Geology, Dibrugarh University, Assam, India

[3]Department of Climate Physics, Pusan National University, Busan, South Korea

[4]Department of Oceans, Rivers, Atmosphere and Land Sciences, Indian Institute of Technology, Kharagpur, India

*Corresponding author: Suchita Pandey, Department of Atmospheric and Ocean Studies, University of Allahabad, Uttar Pradesh, India; E-mail: suchi.rsgis@gmail.com

Abstract

The air-sea interaction processes during the Tropical Cyclone (TC) formation and intensification affect the upper ocean mixing processes thereby changing stratification parameters and vigour of upwelling which ultimately enhances biological activity. Hence the current study conducts a comparative analysis of surface chlorophyll (Chl-a) changes during four tropical cyclones *viz*. Mala (pre-monsoon) cyclone, Nilam cyclone, Phailin cyclone, and Hudhud (post-monsoon) cyclone occurred in the Bay of Bengal (BoB) using numerical modelling. The study depicts the influence of net heat flux and winds on the variability of Chl-a concentration, Mixed Layer Depth (MLD), and Sea Surface Temperature (SST) along the track of the cyclones. Here, we have performed three experiments using Regional Ocean Modelling System (ROMS) coupled with a four-component ecosystem model with daily and climatological forcing for Wind Stress Curl (WSC) and Net Heat Flux (NHF). The first experiment (*viz*. the control run) includes the daily forcing of WSC and NHF during cyclone days. The second experiment comprises only the daily WSC with climatological NHF while the third experiment considers the daily forcing of NHF and climatological WSC. Stratification parameter is estimated for all the three experiments to find out which experiment is well suited for maximum mixing during and post-cyclone periods. The results showed that during Mala cyclone the winds are more effective and play an important role in mixing. The reason for the weaker impact of NHF may be attributed to higher heating over the ocean surface in summer which tends to increase the stratification. The reason may be attributed to NHF, as the flux during post-monsoon season is negative which suggest that ocean surface is warmer which is indicative of a more congenial environment for mixing. On the other hand, it is analysed that the NHF and the WSC play an important role in mixing for the Nilam, Phailin, and the Hudhud cyclones. This implies that in addition to strong WSC, higher heat loss from the ocean surface during winter increases the density of surface waters and the water column becomes convectively unstable leading to vertical mixing and changing the surface Chl-a concentration.

Introduction

One of the most devastating impacts of the air-sea interaction process is formation of Tropical Cyclones (TCs). It causes significant damage to coastal areas thereby leading to significant socio-economic losses. Warm ocean water supplies the surface latent heat flux, which acts as a fuel to cyclogenesis and intensification [1,2]. However, TC formation is important for the oceanic ecosystem and productivity. The Wind Stress Curl (WSC) and Net Heat Flux (NHF), which occur at different stages during the lifetime of a TC affect the Mixed Layer Depth (MLD) in the ocean thereby changing the availability of nutrients at the ocean surface. The TC intensities differ with seasonal variation of the atmosphere and it alters with changing pressure deficit and wind speed. The winds during TC also increase the efflux of Carbon dioxide (CO_2) between the ocean and atmosphere [3]. Therefore, understanding the changes of the Chlorophyll-a (Chl-a) concentrations and the associated mechanisms are important for the global climate and oceanic ecosystem.

Globally TCs may continue to intensify further with increased Sea Surface Temperatures (SST) due to global warming [4,5]. A study by Webster observed an increase in the frequency of category 4 and 5 cyclones for the period 1970-2004 across the globe [6]. Additionally, various studies have also focused on Chl-a increment during cyclone passage across various regions of the global ocean basins. Lin shows that cyclone Kai-Tak triggered the 30-fold increase in Chl-a with 0.8 Mt carbon fixation in the South China Sea (SCS) [7]. Another study by Mei compared SST cooling and Chl-a increment caused by similar TC forcing between SCS and tropical Northwest Pacific Ocean (NWP) [8]. They found that 1.5 times SST cooling and a 10-fold increase in Chl-a occurred in SCS as compare to NWP due to shallower nitracline and stronger vertical nutrient gradient in the SCS. A recent study by Liu and Tang, shows the impact of interactions between Hurricanes and mesoscale eddies on phytoplankton bloom in SCS using nine years (2002-2010) satellite observations [9]. The study depicts a nearly 35%, 6%, 12% increase in Chl-a concentration resulting due to interaction of TCs with cyclonic, anticyclonic, and non-eddy oceanic conditions respectively. Another evidence of phytoplankton bloom after the occurrence of Hurricane Katrina in the Gulf of Mexico is observed in

2005. Turbulent wind mixing is the main source of observed changes in ocean optical and bio-optical properties [10]. A study by Parker over the Great Barrier Reef, Australia showed the relationship between tropical cyclone activity, nutrient loading, and algal blooms [11]. Their research shows that tropical cyclone activity reduces water quality at 8 and 16-day time lag. These relationships suggest that at early stages (during and just after cyclone activity) algal response is induced primarily through wind-driven sediment resuspension. However, wind speed alone only increases minimum levels of Chl-a, rather than mean or extreme upper values. The phytoplankton bloom in response to the cyclonic events is due to upward pumping of nutrients like phosphate and nitrate-rich deep water. Besides, phytoplankton is the regulator of the global carbon cycle and it affects global temperature by modulating SST. Considering that phytoplankton consumes CO_2, it plays a vital role in the air-sea exchange of greenhouse gases. Besides, hurricane-induced impacts on phytoplankton are important for understanding our climate system and the possible consequences of increased atmospheric CO_2 levels, which may include more intense storms.

The Bay of Bengal (BoB) which is located in the north-eastern part of the Indian Ocean has also been experiencing an increase in the frequency of severe to very severe cyclones in recent decades [12-14]. As compared to the Arabian Sea (AS), the BoB is highly vulnerable to cyclones and also it is the basin of low productivity. Hence, in the current study, the influence of cyclones on the productivity of the BOB is considered. The overall coastal zone is an easy target for cyclones and it occurs generally in spring inter-monsoon (April–May) and fall inter-monsoon (October-November) periods [15]. Additionally, the TC activities over BoB are influenced by different climate modes *viz.* El Nino Southern Oscillations (ENSO) and Indian Ocean Dipole (IOD) [16]. The BoB is a unique basin, which is surrounded by densely populated coastal zones from all sides except the south. Another unique feature observed over the BoB is the monsoonal reversal of winds [17]. This basin also receives a huge quantity of freshwater discharge and rainfall during the summer monsoon. The seasonal precipitation, fertile soils, and prominent fisheries are important factors for the dense population in the coastal countries and TCs affect these regions physically as well as economically. Hence the current research aims to understand the relationship of TCs with productivity using the numerical simulation (i.e. sensitivity experiments) over BoB.
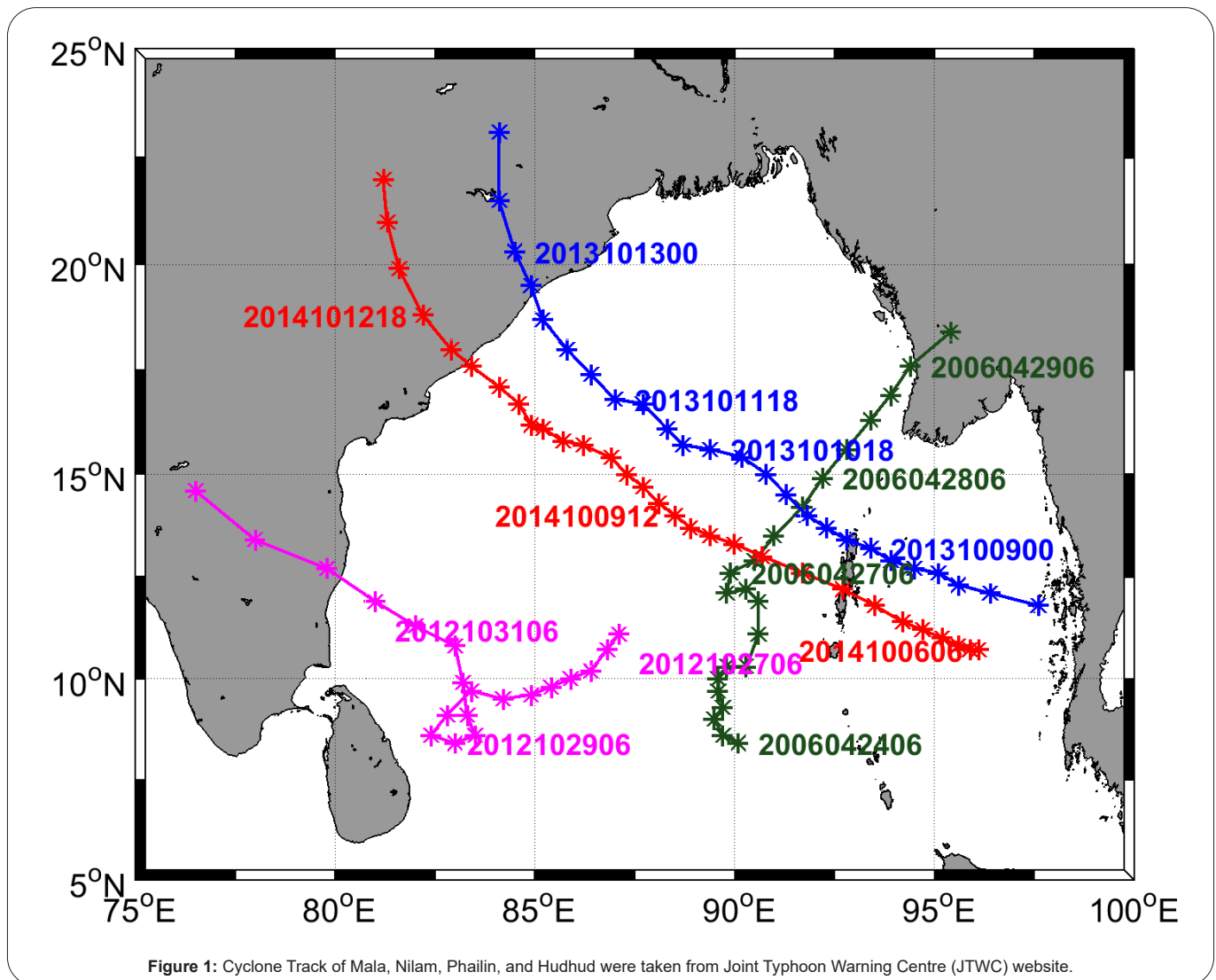
The physical effects of TCs, include a decrease in SST, a deepening of the ocean mixed layer, and upwelling in the wake of the passing hurricane [18-25]. Studies have also shown an increment in Chl-a concentration because of tropical cyclone's passage across the basin [26-29]. Sarangi studied 15 cyclonic storms from 2002 to 2009 in BoB by using MODIS-Aqua and concluded that increase in surface Chl-a concentration from (1.0-5.0 mg/m³) in coastal and offshore waters with a decrease in SST (roughly 2°C) by the effect of the cyclone [30]. Another study by Chacko and Zimik observed that the upper 40 m of ocean subsurface experiences warming while the cooling occurs below 40-80 m during the Thane cyclone (2011) in BoB [31]. They also found that two upwelling regions attributed to Ekman pumping velocity, slow translation speed, and the availability of nitrate concentration in the shallow coastal waters. Similarly, Krishna found that more intensified cyclones attributed higher Chl-a concentration with significant cooling of the oceanic surface than a less intensified cyclone, due to differences in their intensities and translational speeds [32].

Although past studies have documented a measurable increase in Chl-a concentrations as a result of TCs, the magnitude of this increase relative to the physical processes that impact ocean Chl-a needs to be assessed to understand the consequence of increasing TC frequency and/or intensity for ocean biology and chemistry of BoB. Neetu depicted that upper ocean stratification has a significant impact on TC-induced surface cooling [33]. The study reported almost three times higher surface cooling during pre-monsoon TCs than post-monsoon TCs, which is attributed to seasonal changes in stratification rather than winds. Keeping this in view, the present study investigates the effect of winds and NHF during the cyclone period on stratification and associated mechanisms in the BoB by conducting numerical experiments using Regional Ocean Modelling System (ROMS) simulations. The current research aims to understand the variability of Chl-a concentration with cyclones of varying intensities and its driving physical parameters. For this particular study, four cyclones are chosen, one occurring in the pre-monsoon period while others in the post-monsoon period. Details of the cyclones are given in Table 1 and tracks are shown in Figure 1.

The following section of the paper includes model setup, methodology, and validation. Model performance includes a biological response, followed by the response of mixed layer depth. The next section includes results, discussion, and conclusion.

Table 1: Details of the cyclones considered for the present study.

Cyclone	Year	Seasons	Category		Min. Press (hPa)	Max. Wind		Peak
						Speed (km/h)		
			IMD Scale	Saffir-Simpon Scale		(3 min. sustained)	(1 min. sustained)	Intensity
Mala	Apr 24-30, 2006	Pre monsoon	Extremely severe cyclonic storm	Category-4	954	185	220	28-Apr
Nilam	28Oct-1Nov, 2012	Post monsoon	Cyclonic storm	Tropical Storm	990	85	100	31-Oct
Phailin	Oct 5-14, 2013	Post monsoon	Extremely severe cyclonic storm	Category-5	940	215	260	11-Oct
Hudhud	Oct 8-14, 2014	Post monsoon	Extremely severe cyclonic storm	Category-4	950	185	215 (Gusts:260)	12-Oct

Figure 1: Cyclone Track of Mala, Nilam, Phailin, and Hudhud were taken from Joint Typhoon Warning Centre (JTWC) website.

Methodology

Model setups

To decipher the impact of the cyclonic activity on productivity, 'Regional Ocean Modelling System' (ROMS) AGRIF version 2.1 is used. At first, the climatological run is carried out for 10 years with a time step of 600 seconds. Model is forced with tides (all major ten components), river runoff with major rivers of BoB (Padma, Brahmaputra, Meghna, Irrawaddy, Godavari, Mahanadi, and Brahmani), atmospheric forcing's, and air-sea fluxes. ROMS-AGRIF is a high resolution, free surface, terrain-following ocean model, which uses a split-explicit time step algorithm to obtain mathematical feedback between the baroclinic momentum and tracer equations and the barotropic momentum and continuity equations [34]. The model uses a curvilinear coordinate system in the horizontal and sigma coordinate system in the vertical with an Arakawa C grid scheme.

The model domain extends from 4°N-24°N and 76°E-100°E, with open boundary conditions except for north (Figure 2). The open borders help to incorporate the remote forcing by interpolating the climatological variables from the southern side of the BoB. The horizontal grid resolution is 1/6° (approx. 16 km), with a grid size of 143 in the zonal and 124 in the meridional directions. There are 32 vertical layers used in the current simulations (Figure 2). The vertical parameters *viz.* vertical s-coordinate surface control parameter (theta s) is put as 7.0, s-coordinate bottom control parameter (theta b) is 0.1, and Tcline depth (Thermocline) of 10 m can resolve the mixed layer stability obtained from the Brunt Vaisala frequency at different parts of the BoB using the K-Profile Parameterization (KPP) scheme for vertical mixing [35]. The first nine years of simulation are considered as spin-up years and the simulation results from the tenth year (obtained after stabilization of model kinetic energy) have been used in the present study to do the sensitivity experiments with WSC and NHF. Initial conditions for the experiments are obtained from the final year climatological spin-up simulation. Three experimental test runs are carried out for each cyclone case. The first test run (Exp-1) is the control run in which daily forcing of WSC and daily forcing of NHF with climatological forcing's for other variables is used. In the second test (Exp-2) run only daily forcing's of WSC is used with climatological spin up. The third experiment (Exp-3) includes the daily forcing of NHF with climatological spin up.
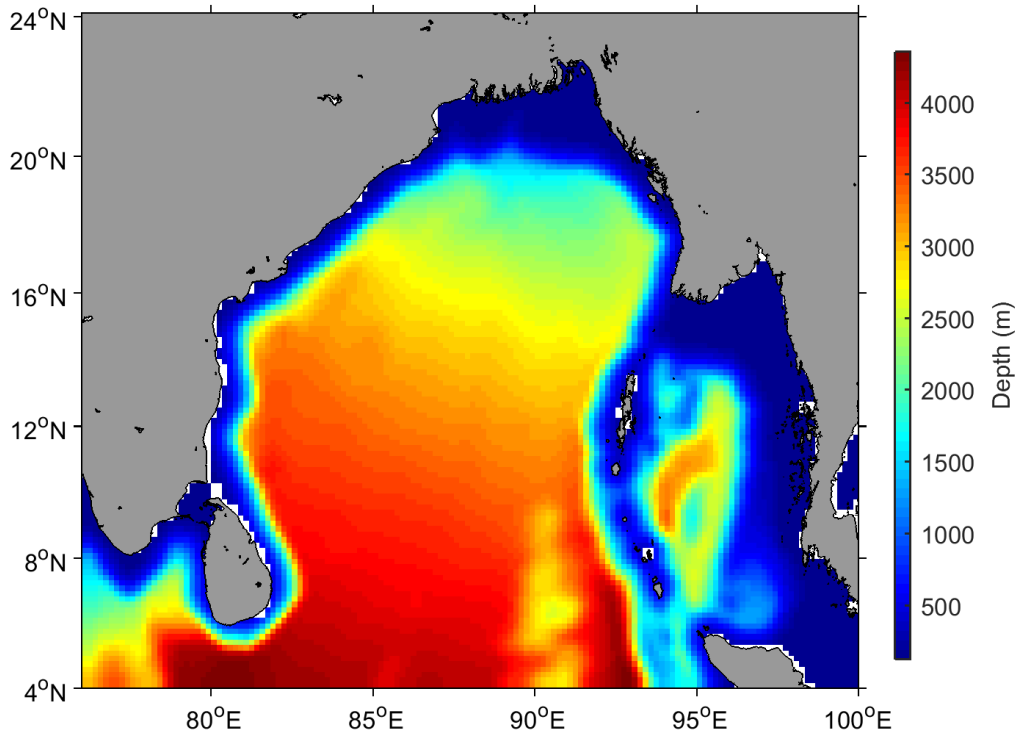
Figure 2: Model domain extending from 5°S-30°N and 40°E-100°E showing only northern boundary closed and remaining eastern, western, and southern boundaries open. The color shades depict the bathymetry with the depth varying from 1000 m on the north side to above 4500m on the south side.

Ecosystem model

In the present study, ROMS is coupled with a four-component NPZD ecosystem model. The model components include Nitrate, Phytoplankton, Zooplankton, and Detritus (NPZD) with single limiting nutrients as nitrogen and single phytoplankton operational type. The model includes an arrangement, of seven coupled partial differential equations that include nitrate, ammonium, detritus, phytoplankton, zooplankton, and an active phytoplankton carbon to chlorophyll ratio. All these scalar quantities are advected and diffused at the rates as determined by the model ROMS. Sinking is allowed for phytoplankton, with most of the movement of particulate mass associated with the sinking of larger particles. The equations that describe the flow of nitrogen among various biological pools are obtained from Fasham [36]. The model equation for the four-component NPZD biogeochemical model is given below:

$$\frac{d[NO_3]}{dt} = -t_{PP\max} \cdot Q_{NP} \cdot [Phyto] \quad \ldots\ldots(1)$$

$$\frac{d[Phyto]}{dt} = t_{PP\max} \cdot (Q_{NP}) \cdot [Phyto] - t_{Pmort} \cdot$$

$$[Phyto] - Q_{graze} \cdot [Zoo] - L_{vp} \frac{\partial[Phyto]}{\partial z} \quad \ldots(2)$$

$$\frac{d[Zoo]}{dt} = Q_{graze} \cdot AE_N \cdot [Zoo] - (t_{Zbmet} + Q_{excr}) \cdot [Zoo] - t_{Zmort} \cdot [Zoo]^2 \quad \ldots(3)$$

$$\frac{d[Det]}{dt} = Q_{graze} \cdot (1 - AE_N)[Zoo] + t_{Pmort} \cdot [Phyto]$$

$$+ t_{Zmort} \cdot [Zoo]^2 - t_{Dremin}[Det] - L_{vd} \frac{\partial[Det]}{\partial z} \quad \ldots(4)$$

The functions used in equations from 2.10 to 2.13 are:

$$Q_{NP} = \frac{[NO_3]}{K_{NO_3} + [NO_3]} \quad \ldots\ldots(5)$$

$$Q_{graze} = t_{Zgraze} \cdot \frac{[Phyto]}{K_P^2 + [NO_3]} \quad \ldots(6)$$

Where, KNO_3 is the Half-saturation concentration for uptake of NO_3 and K_P is the

Half-saturation concentration for zooplankton grazing.

$$t_{PP\max} = f(PAR) = \frac{V_P . \alpha . PAR}{\sqrt{V_P^2 + \alpha^2 PAR^2}} \quad \ldots(7)$$

The evolution of nitrate, phytoplankton, zooplankton, and detritus concentration is determined from equations 1 to 4. The variables used in equation 1 to 7 are described as follows, such as, the variables t_{Pmort}, L_{vp}, t_{pp} represents phytoplankton mortality rate, sinking speed and growth rate respectively; T_{Zgraze}, AE_N, t_{Zbmet}, Q_{exert}, t_{Zmort} represents zooplankton grazing rate, grazing efficiency, metabolism rate, excretion rate and mortality rate respectively; L_{vp} is detritus sinking speed; K_{NO_3} and K_P are Half-saturation concentration for uptake of NO_3 and zooplankton grazing respectively; V_P is the maximum growth rate; PAR is photo synthetically available radiation whereas function $f(PAR)$ is Photosynthesis-light (P-I) relationship and $\acute{a}$ is the initial slope of PI curve [37,38]. Here, the biogeochemical components are coupled to ROMS as these aids in providing the initial conditions and lateral boundary conditions for the NPZD model.

Biological parameters used in model run are listed in Table 2.

Table 2: Description of biogeochemical parameters used in the model run.

Parameter Considered	Symbol Used	Value	Unit
Growth rate of maximum phytoplankton concentration	VP	f(T)	d^{-1}
Half saturation concentration considered for nitrate uptake	KNO_3	0.5	mmol NM^{-3}
Mortality rate of phytoplankton	tPmort	0.01	d^{-1}
Photosynthetic index	A	0.7	mol $CgChl^{-1}$
Sinking rate of phytoplankton	Lvp	0.1	md^{-1}
Efficiency of grazing	AEN	0.7	-
Half saturation concentration considered for zooplankton grazing	KP	0.5	mmol NM^{-3}
Basal metabolism caused by excretion rate	tZbmet	0.007	d^{-1}
Highest rate of assimilation associated with excretion	Qexcr	0.007	d^{-1}
Re-mineralization rate of detritus	tDrimin	f(T)	d^{-1}
Mortality rate of zooplankton	tZmort	0.006	d^{-1}
Sinking rate of detritus	Lvd	1	md^{-1}

Data and methods

The initial conditions for temperature, salinity, nitrate, phosphate, oxygen, and silicate are set by using World Ocean Atlas (WOA 2009) data. Data of Chl-a, climatological wind, and atmospheric forcing are obtained from SeaWiFS, QuickSCAT, and COADS05 respectively. ROMS model is coupled with the four-component ecosystem model (discussed in section 2.2). After the stabilization of volume-averaged kinetic energy, the tenth-year spin-up results were used as initial conditions for the three experimental test runs which are carried out separately for each cyclone with daily cyclonic physical forcing's. Similarly, the observation data of the temperature and salinity are taken from Argo floats in the vicinity along the track of cyclone to estimate the MLD and Barrier Layer Thickness (BLT). The Chl-a data is from Copernicus-Glob Colour products with a spatial resolution of 4 km × 4 km and one-day temporal resolution. These products are global continuous daily cloudless fields of chlorophyll (based on an Optimal-Interpolation approach) and the sensors used are SeaWiFS, MODIS-Aqua, MERIS, VIIRSN, and OLCI-S3A. The zonal velocity (U) that is the component of horizontal wind towards East and the meridional velocity (V) that is the component of horizontal wind towards North. U wind and V winds components (in m/s) are obtained from QuickSCAT. The spatial resolution is 0.25 degrees and the temporal resolution is one day. Net heat flux data for Mala cyclone is obtained from Objectively Analysed Air-Sea Fluxes (OA Flux) of WHOI. Net heat flux data (Qnet) for Nilam, Phailin, and Hudhud are estimated from Short Wave (SW), Long Wave (LW), Sensible (SH), and Latent Heat (LH) by using the relationship: Qnet=SW-LW-LH-SH. These data are obtained from the Modern Era Retrospective-analysis for Research and Applications (MERRA) at daily temporal resolution and 1/2˚ × 2/3˚ spatial resolution Apache HTTP server. Sea Surface Temperature (SST) data is taken from Apache HTTP server with a temporal resolution of one day and spatial resolution of 0.25˚. The National Geospatial Data Asset (NGDA) high resolution SST analysis products have been used. The products use data from both the sensors Advanced Very High Resolution Radiometer (AVHRR) and Advanced Microwave Scanning Radiometer from NASA Earth Observing System (AMSR-E). Argo data is from the Indian National Centre for Ocean Information Services (INCOIS). The spatial resolution of Argo MLD is 1˚ × 1˚ and it is obtained after every 10 days interval. The cross-section in the model along the 12˚ N latitude showed the depth of the sigma levels (Figure 3). Cyclone track data has been obtained from Regional Specialised Meteorological Centre (RSMC)-Tropical Cyclones, IMD, and New Delhi.

Upper ocean characteristics in response to the tcs

Spatial biological response: Mala was the strongest tropical cyclone of the year 2006 and it started on April 24th, attains maximum speed on April 28th, and dissipated on April 30th. As the cyclone progresses the surface Chl-a increases along the track of the cyclone. The spatial extent of Chl-a in BoB before, during, and after the cyclone, Mala along with the standard deviation for the lifetime of the storm is shown in Figure 4. There is an increase in the surface Chl-a concentration along the track during and after the passage of the storm. The maximum standard deviation of Chl-a, is also found around 15˚N and 93˚E, along the track of Mala cyclone. The standard deviation plot depicts the increased Chl-a, which occur during the passage of the TCs with most regions of increased productivity being on the right of the track as the TC progressed towards land.

The period of 5 days has been considered for the study of different parameters as before, during and after the cyclone. As the Mala started on 24 April and dissipated on 30 April. Hence the five days before (April 19 to April 23) the cyclone occurrence, five days during the cyclone (April 25 to April 29) and five days after (May 1 to May 5) the dissipation of the cyclone has been chosen for the study. The standard deviation has been computed for the period considered as during the cyclone (April 25 to April 29).

The TC Nilam occurred in the year 2012 which was initiated on October 28th and attains high wind speed of 85 km/h on October 30 after which it made landfall on October 31st near Mahabalipuram (12.6˚N, 80.2˚E), Tamil Nadu. Chl-a enrichment can be seen during and after the cyclone (Figure 5). The standard deviation (calculated for during the cyclone) plot depicts the increased Chl-a which occur during the passage of the TCs with most regions of increased productivity being on the coastal region of Sri Lanka as the TC progressed towards land
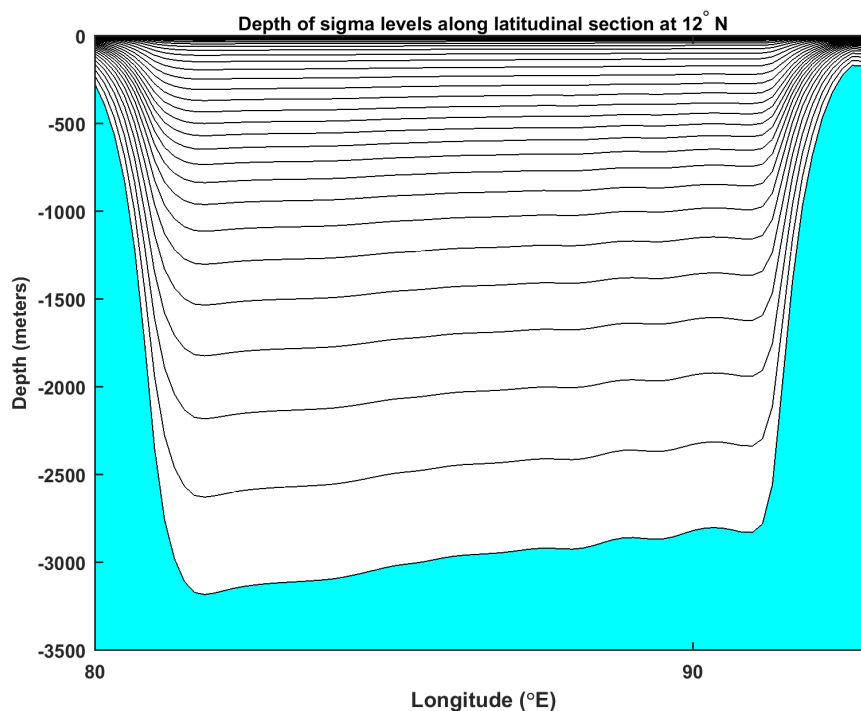
Figure 3: The model cross-section along the 12°N latitude showing the depth of vertical sigma levels. Note: The model resolution increases as the thickness decreases to resolve mixed layer stability.
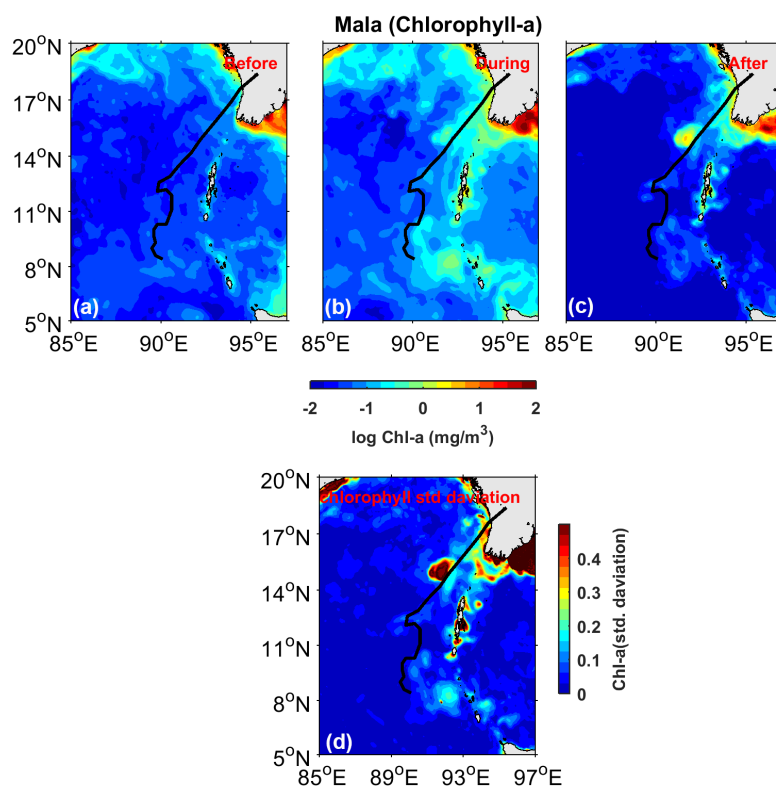

Figure 4: Chl-a pigment concentration from satellite observations (a) before(b) during (c) after the Mala Cyclone, and (d) the standard deviation of Chl-a during the cyclone, from April 25th to April29th 2006.
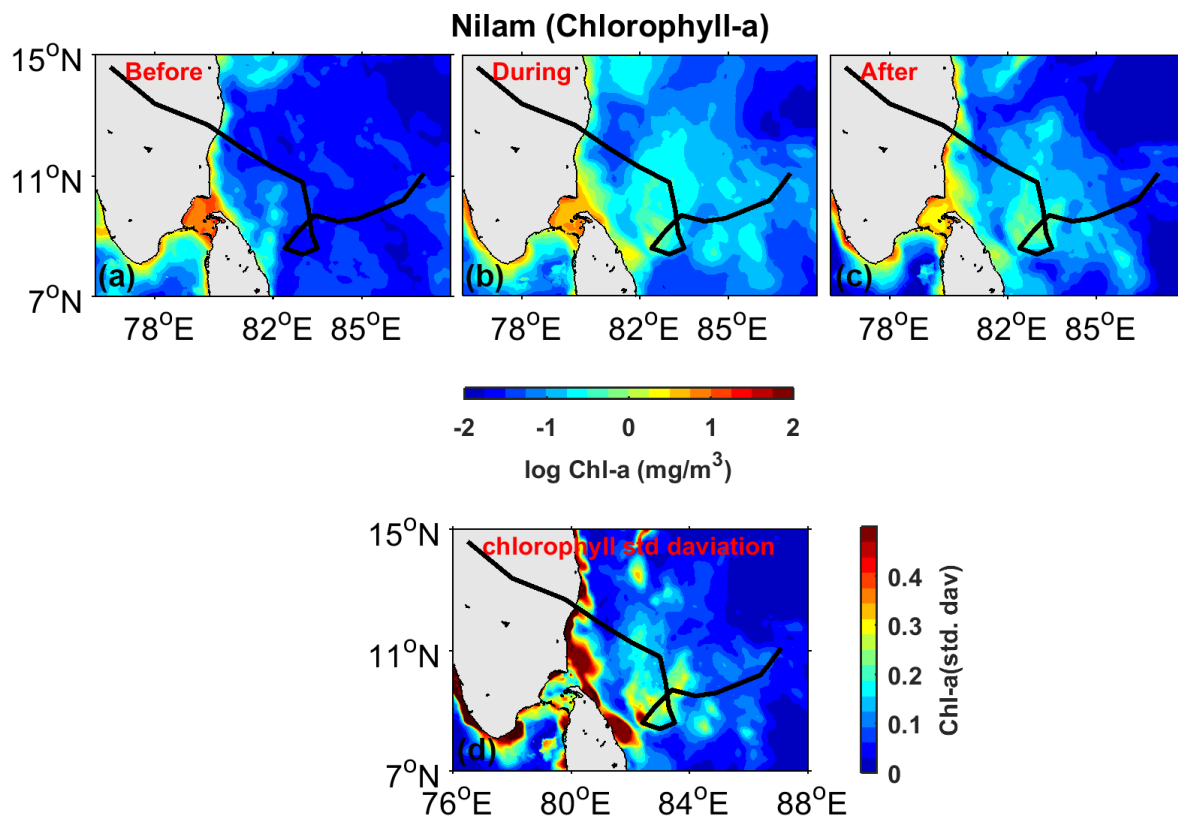
Figure 5: Chl-a pigment concentration from satellite observations (a) before (b) during (c) after the Nilam Cyclone, and (d) the standard deviation of Chl-a from October 28th to November 1st 2013, during the cyclone.

Similarly, for Nilam cyclone, it started on October 28 and dissipated on November 1. So the cyclone persists for 5 days. Hence period chosen for analysis as before, during and after the cyclone is 5 days. The five days before (October 23 to 27) the cyclone occurrence and five days after (November 2 to November 6) the dissipation of the cyclone has been chosen for the study. The standard deviation has been computed for during the cyclone (October 28 to November 1).

Phailin is an extremely severe cyclonic storm initiated on October 4th and got its peak on October 11th. The highest winds during the cyclone was 115 Knots (IMD-RSMC-Best Track Data). Similar to the previous cyclones, (Figure 6) shows that an increment in the surface Chl-a concentration along the track of the storm as it intensified. The rate of increment of Chl-a concentration slows down after the landfall of the storm on October 13th near Gopalpur, Odisha. The standard deviation (during the cyclone) depicts that the regions of high productivity with increased Chl-a concentration found on the right side of the track as the cyclone progresses towards land.

Again the Phailin cyclone resides from October 4 to October 14 and it continued for 11 days. The 5 days before (September 29 to October 3) the cyclone occurrence, 5 days during the cyclone (October 8 to October 12) and five days after (October 15 to October 19) the dissipation of the cyclone has been chosen for the study. The standard deviation has been computed for the period considered as during the cyclone (October 8 to October 12).

Hudhud is also an extremely severe cyclonic storm that initiated

on October 7th, 2014, and reached its maximum intensity on October 12th with maximum wind speed of 100 Knots. Finally, it made landfall near Visakhapatnam on October 14. Hence the duration of Hudhud cyclone is five days (October 8 to October 12) has been considered for during cyclone study. Hence five days' period has been chosen for before (October 2 to October 6) and five days after (October 15 to October 19) analysis. Figure 7 shows the spatial extent of surface Chl-a concentration from observations with an increase in surface Chl-a value during and after the passage of the cyclonic storm. The standard deviation (during the cyclone, October 8 to 12) depicts an increased Chl-a, during the passage of the TCs with most regions of increased productivity being along the track as the TC progressed towards land.

The daily Chl-a concentration derived from satellite data for all the cyclones are averaged within 2° × 2° of spatial region along the track of the cyclone. The increment of Chl-a is calculated by the difference of the values after and before the passage of the cyclone. The along-track box-averaged values of daily Chl-a concentration are presented in Figure 8a, which also shows the duration of the period taken for Mala cyclone before (April 19 to April 23), during (April 25 to April 29) and after (May 1 to May 5). Mala which is designated as an extremely severe cyclonic storm with maximum wind speeds attained on April 28th of 2006, where maximum concentration was 0.4 to 0.7 mg/m³ (Table 1 and Figure 8a). The increment of Chl-a concentration before and after a cyclone is 0.7 mg/m³ and the increase from during and before the cyclone is 0.7 mg/m³.
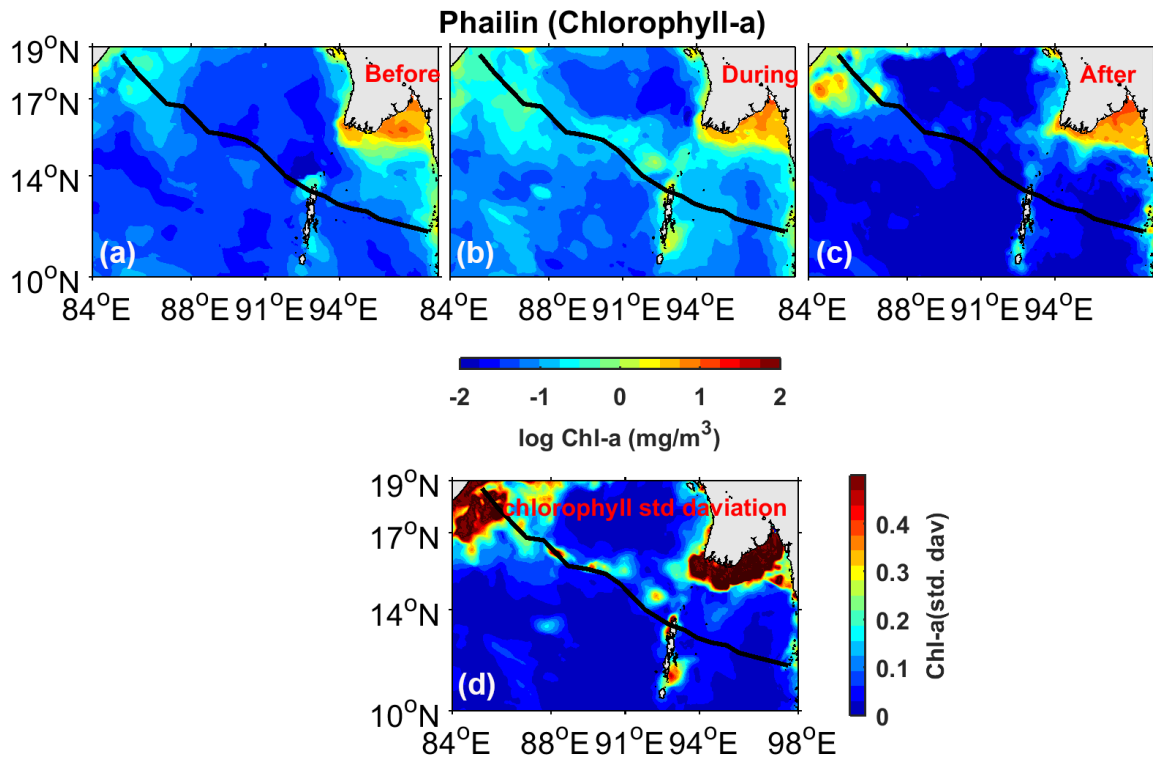
Figure 6: Chl-a pigment concentration from satellite observations (a) before (b) during (c) after the Phailin Cyclone and (d) the standard deviation of Chl-a, from October 8th to October 12th 2013 during the cyclone.
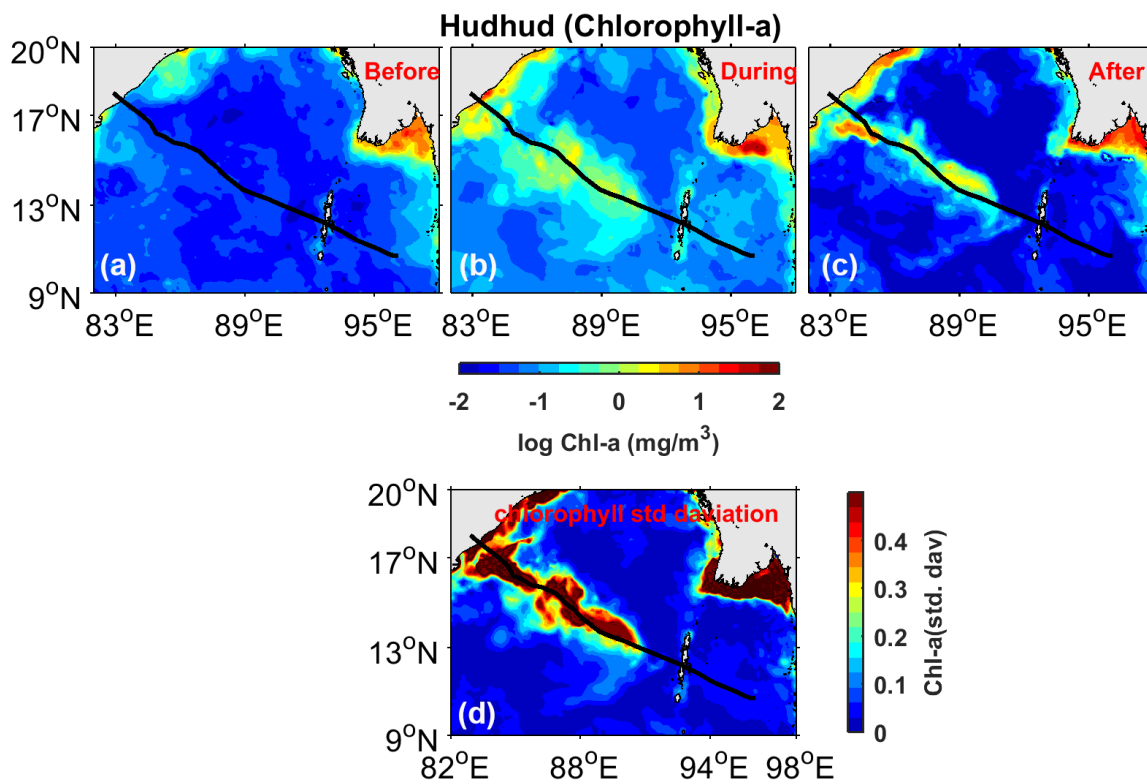

Figure 7: Chl-a pigment concentration from satellite observations (a) before (b) during (c) after the Hudhud Cyclone, and (d) the standard deviation of Chl-a form October 8th to October 12th 2014, during the cyclone.
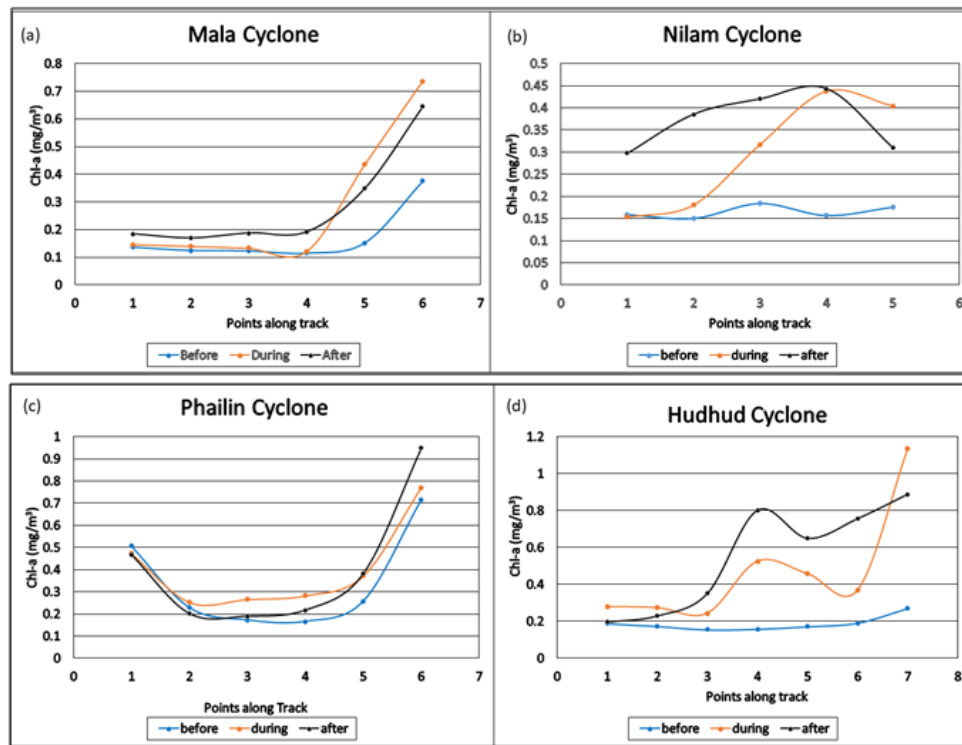
Figure 8: Comparison of satellite-derived Chl-a for before, during, and after the cyclone Mala, Nilam, Phailin, and Hudhud. Note: before (━━━); during (━━━); after (━━━).

Figure 8b shows that the box-averaged observed Chl-a values along the track of the Nilam cyclone before (October 23 to 27), during (October 28 to November 1), and after (November 2 to November 6). It reaches its maximum speed on October 31st, 2012 with a maximum value of Chl-a was 0.44 mg/m³ between 11° to 13° N and 79° to 82°. The overall increment (along the track) of Chl-a between after and before the cyclone is 1.03 mg/m³ and the increment from during and before is 0.66 mg/m³.

At the right side of the cyclone the SST changes is abrupt which affect the mixing hence due to heat loss, evaporation and wind stirring hence the deep cold nutrient rich water comes up and MLD increases while barrier layer becomes shallow as shown in subsequent figures. Subsequently the Chl-a concentration becomes high on the ocean surface at the right side of the cyclone.

Figure 8c shows the daily box-averaged Chl-a concentration for Phailin cyclone derived from satellite observations before (September 29 to October 3), during (October 8 to October 12), and after (October 15 to October 19). The maximum Chl-a concentration is found on October 12th (during) and October 19th (after) with the value of 0.4 mg/m³ and 0.8 mg/m³ having a latitudinal/longitudinal extent of 11°N to 13°N and 96°E to 98°E and 17°N to 20°N and 84°E to 87°E respectively. The increment in Chl-a form after the cyclone to during cyclone is 0.36 mg/m³ and from during cyclonic event to before event is 0.37 mg/m³.

Figure 8d shows the box-averaged values of observed Chl-a concentration for the Hudhud cyclone before (October 2 to October 6), during (October 8 to October 12), and after (October 15 to October 19). The maximum daily Chl-a concentration along the track

is 0.6 mg/m³ and 1.14 mg/m³ during the cyclone on October 9th and October 12th respectively. The latitude and longitude of maximum Chl-a are 13°N to 15°N and 88°E to 80°E and 17°N to 19°N, 82°E to 84°E for during the cyclone. The increment in Chl-a concentration in the duration of after and before the cyclone is 2.6 mg/m³ and during and before cyclone is 2 mg/m³. The comparative analysis of surface Chl-a concentration observed during different TCs (Figure 8), depicts that very intense cyclones (*viz.* Hudhud, Phailin) have high Chl-a concentration compared to Nilam. All these three TCs represent post-monsoon cyclones with different intensities. The concentration of Chl-a is more in Hudhud and Phailin as compare to Mala. On the other hand, the concentration of Chl-a is more in Mala cyclone than the Nilam cyclone (for before, during and after the cyclone period). The fresh water influx during the post-monsoon season increases sea surface temperatures and upper ocean heat leading to more intense cyclones in that season compared to the pre-monsoon season [39]. The more intense the cyclones, the higher increment in the surface Chl-a concentration values.

Following this, we illustrate the comparison of Chl-a values of the three model experiments (Exp-1: With daily wind stress forcing and daily net heat forcing; Exp-2: With daily wind stress only; Exp-3: Daily net heat forcing only) with satellite observations along the track of the Phailin cyclone. The model simulated Chl-a values are overestimated at some specific points along the track. The same points were taken before, during, and after the cyclone along the track. The first model experiment shows maximum Chl-a values than the other two experiments. The model derived Chl-a values that reach up to 1.3 mg/m³ while the observation values of Chl-a reach up to 1 mg/m³. It shows a comparable trend in Chl-a concentration in different

experiments with the satellite observations. Similar results are found for other three cyclones across the BoB region. The daily observations of Chl-a shows reasonable similarity with the model simulated values before, during, and after the cyclone by inducing the daily forcing of net heat flux and wind stress curl.

As discussed in the later sections (section 3.2 and 3.3) the strong winds on the right side of the track of the cyclone enhance the turbulence by mechanical stirring and vertical shear, hence vertical mixing increases which deepened the mixed layer and eroded the barrier layer. Hence the mixed layer deepened and barrier layer thins or vanishes in some cases.

Response of mixed layer depth: A quasi-homogeneous region in the upper ocean where there is little variation in temperature or density with depth is considered as ocean mixed layer depth. It can be defined by the temperature and the density. The temperature defined mixed layer, DT-0.2, is defined as the depth at which the surface temperature cools by 0.2°C. The density defined mixed layer, Dsigma, is 40 m and described as the surface density plus the density difference brought about by the temperature increment of 0.2°C.

During cyclones we observe intense winds which lead to the vertical mixing over the oceanic regions across the global ocean basins. This mixing increases the mixed layer depth by few meters depending on the stratification of the ocean. Therefore, we estimate the Mixed Layer Depth (MLD) which is then averaged within the 2˚ × 2˚ spatial box along the track of the cyclone, for all four cyclones, as shown in Figures 9 and 10. The observed MLD is derived from the Argo data and in the model, the mixed layer thickness defined by mixing scheme is considered as the MLD. The MLD increases during and after the cyclone period which is observed in both Argo observations and model simulation. The MLD increases by 40 m during the Mala cyclone. MLD ranges from 40 to 50 m during (October 30, 2012) and after (November 10, 2012) for the cyclone Nilam as seen from model and observation. In the case of the Phailin cyclone, the Argo MLD increases as 50 m (October 10, 2013) during the cyclone while it decreases to 28 m after (October 20, 2013) the cyclone and the model

simulated MLD is comparable with observation. For Hudhud cyclone, the Argo MLD is less before the cyclone but increases during and after the cyclone. The MLD increases by 38 m and 62 m during the cyclone on October 9 and October 14, 2014, respectively. The MLD range after the cyclone period is 47 m on October 19, 2014. The model-derived MLD is comparable to the observed MLD using Argo data. It shows that the stronger winds during the cyclone which initiates mixing and upwelling of nutrients persists after several days of the cyclone passes. These effects are well captured by the ROMS model across the BoB region during the passage of different intense cyclonic storms.

Results

In order to understand the processes of enhanced Chl-a concentrations during passage of TCs, it is necessary to compare the Chl-a concentration with different parameters which are related to TC formation and intensification (*viz*. Wind stress curl, Net heat flux, SST and Upper Ocean Mixing). Also it discusses the dynamics associated with stratification of the ocean which can lead to identify more productive regions. The following sections elaborate on these aspects.

Response of wind stress curl and net heat flux with Chl-a

In this section, we try to compare the observed variations in Chl-a concentration with Chl-a values from wind stress curl and net heat flux. There is an increase in WSC as well as Chl-a concentration during cyclone as compared to the pre-cyclone values. Also, we observe a phase lag between Chl-a and the WSC increments (Figure 11).

In the case of net heat flux, there is a net negative heat flux just before the initiation of the cyclone due to the transfer of heat from the ocean to the atmosphere. After this, the heat flux again increases leading to the gradual warming of the ocean surface. As the heat flux gradually increases, Chl-a also increases (Figure 12). Thus, it can be inferred that WSC forcing alone is not sufficient, as cooling due to net heat slows down the upwelling process at the initiation stage of the cyclone. But the combined effect of WSC and net heat results in a sharp increase in Chl-a during the cyclone passage.
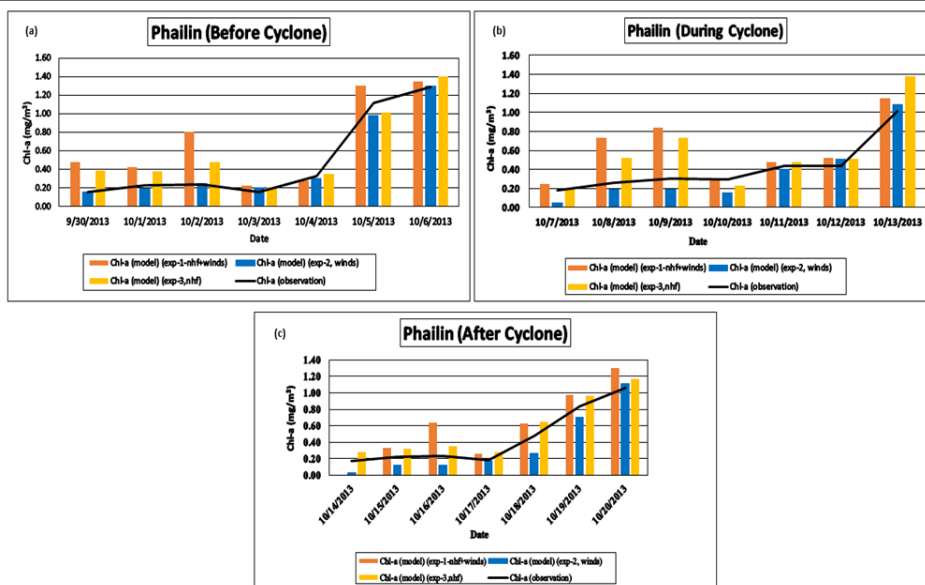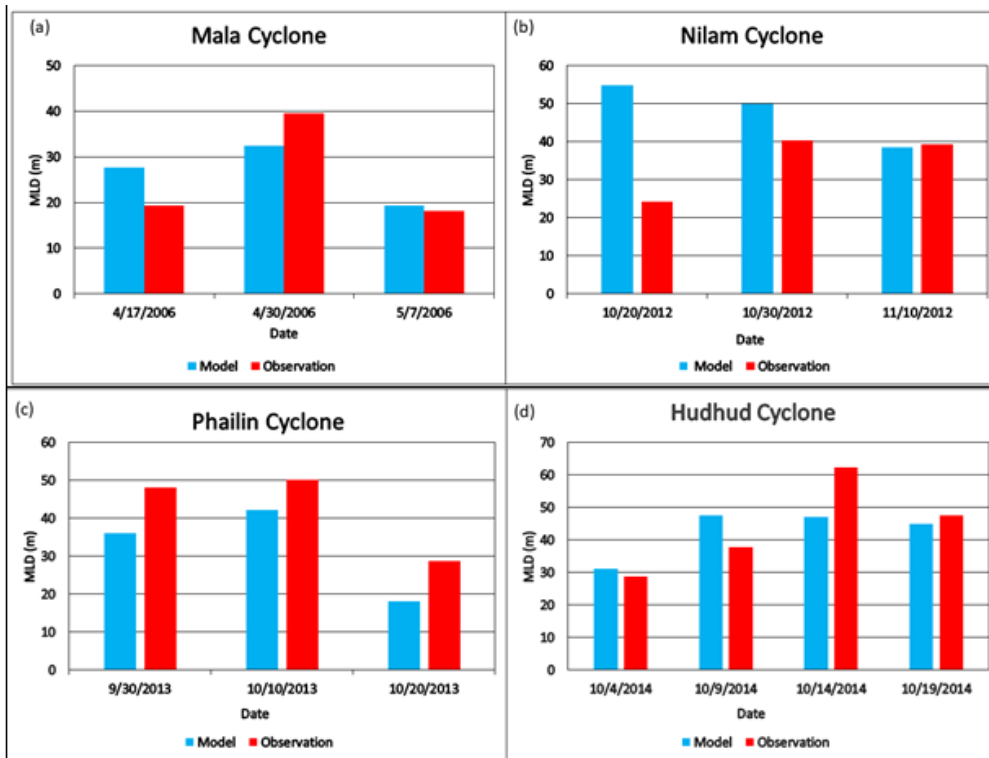

Figure 9: Comparison of Chl-a derived from satellite observation and all three simulation experiments. The first experiment is the control run with climatology and daily forcing of winds and NHF. The second experiment with climatology with daily cyclonic winds and the third experiment represents daily cyclonic NHF forcing with climatology. Note: Chl-a (model) (exp-1 nhf+winds) ( ); Chl-a (model) (exp-2, winds) ( ); Chl-a (model) (exp-3, nhf) ( ); Chl-a (observation) (━).

Figure 9: Comparison of Chl-a derived from satellite observation and all three simulation experiments. The first experiment is the control run with climatology and daily forcing of winds and NHF. The second experiment with climatology with daily cyclonic winds and the third experiment represents daily cyclonic NHF forcing with climatology. Note: Chl-a (model) (exp-1 nhf+winds) (▬); Chl-a (model) (exp-2, winds) (▬); Chl-a (model) (exp-3, nhf) (▬); Chl-a (observation) (▬)..
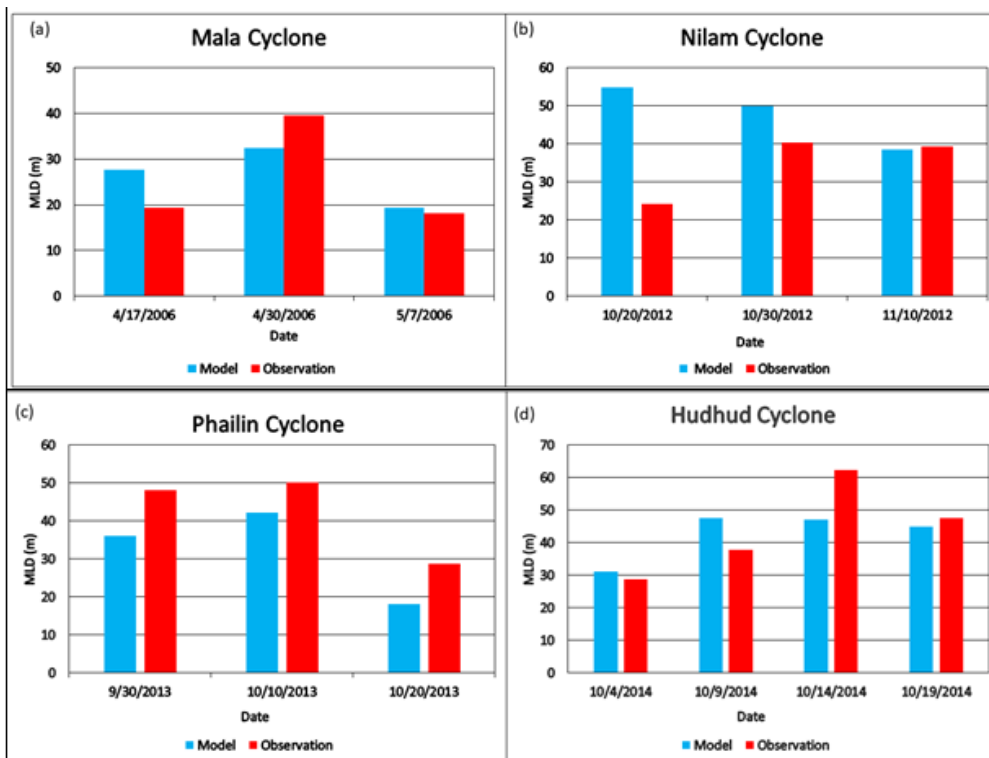

Figure 10: The Mixed Layer Depth (MLD) along the 2°× 2° spatial grid along the track of the cyclone for before, during, and after the cyclone (A) Mala, (B) Nilam, (C) Phailin, and (D) Hudhud. The data represent the Argo MLD and model control run simulated MLD. Note: Model (■); Observation (■).
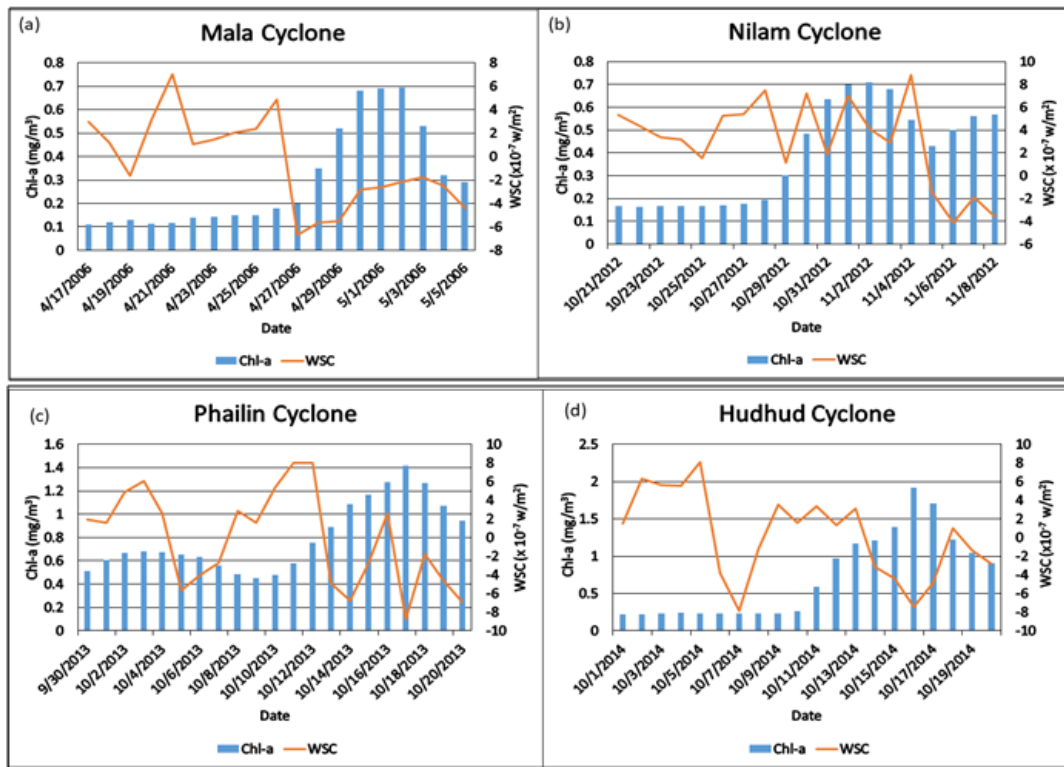
Figure 11: Comparison of Winds Stress Curl (WSC) with Chl-a concentration for (a) Mala (b) Nilam (c) Phailin (d) Hudhud. Note: Chl-a (▮); WSC (▬).
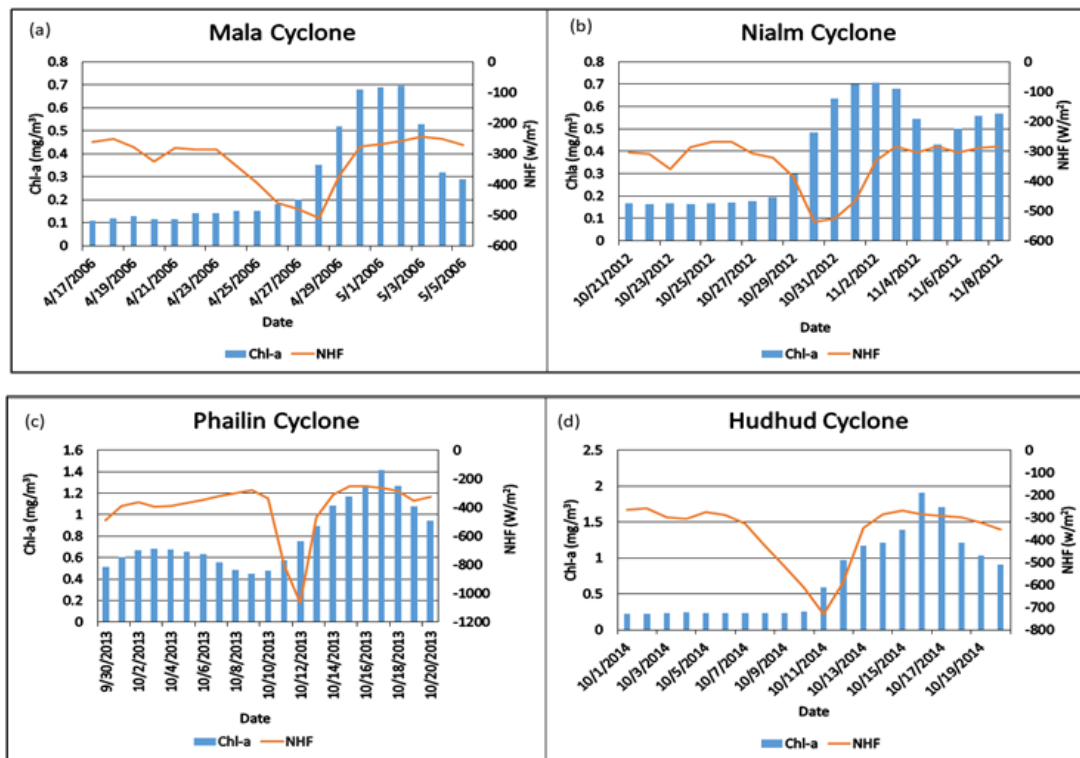

Figure 12: Comparison of Net Heat Flux (NHF) with Chl-a concentration for (A) Mala (B) Nilam (C) Phailin (D) Hudhud. Note: Chl-a (▮); NHF(▬).

Response of SST with Chl-a

SST reduces during and after the passage of a cyclonic storm due to the vertical mixing by bringing the cool sub-surface waters to the surface [40]. The current study observes differences in the magnitude of SST response during and after each cyclone as the SST decreases during and after the cyclonic event. The SSTs drop by 2℃ during the cyclone Mala from May 24 to May 29. It is dropped from 30℃ to 28℃ and it continues to reduce further after the passage of the cyclone. The overall cooling during Mala is between 3℃ to 4℃ along the track of the cyclone. There is a drop of 1.5℃ in SSTs during the cyclone Nilam.

SSTs drop by 1℃ during the Phailin cyclone and cooling of 3℃ persists after the cyclonic event. For Hudhud cyclone, 2℃ drop in SST is noticed during the cyclone and around 7℃ to 8℃ cooling was shown along the track of the cyclone after the cyclonic event (Figure 13). During and after the cyclone the daily satellite observations showed that the SST cooling and increment in Chl-a occurred within $2° \times 2°$ spatial buffer along the track of the cyclone. The maximum cooling occurred with maximum increment in Chl-a during and after the Hudhud cyclone. This shows that there is a variation in the reduction of SSTs with seasons and intensity of cyclones.

For the cyclogenesis the upper ocean heat content is the main oceanic parameter. The depth of the thermocline determines the potential heat content that the ocean could hold in the surface and is being modulated by the planetary waves [41-43]. The propagating down welling (upwelling) coastal Kelvin waves and their associated radiated Rossby waves deepen (shallow) the thermocline in the coastal and central BoB respectively. The central Bay of Bengal region, have the two phases of cyclogenesis, the first and second phase which corresponds to the first and the second down welling Kelvin wave respectively. During the period of down welling Kelvin wave, the thermocline over most part of the BoB is deep corresponding to the dominant positive SSHA. The southern BoB is also dominated by the second upwelling Kelvin wave and it's radiated Rossby waves, whereas the central BoB is dominated by down welling Eddies [44].

Similarly in the study of Nargis cyclone by Mc Phaden analyzed the combined impact of the cyclone on SST from enhanced ocean mixing and turbulent heat loss to the atmosphere was a 2℃–3℃ drop in surface temperature [45].

Response of MLD and BLT with Chl-a

After the formation of a cyclone, the associated strong wind-stress curl drives the upward Ekman pumping, and the resultant entrainment and mixing cool the upper ocean [46-48]. The Nargis cyclone and showed that the anti-cyclonically rotating winds to the right of a moving storm resonantly force inertial oscillations that produce strong vertical current shears and flow instabilities, which are an additional source of turbulence. Thus, enhanced vertical mixing associated with Nargis deepened the surface mixed layer and eroded the barrier layer in the central Bay. The resulting entrainment of cold, high-salinity water from the thermocline lowered SST and increased surface salinity.

The nutrient-rich cool water gains the phytoplankton bloom and leads to the eutrophic condition. In the following section, we analyse the mixing due to Ekman pumping and its effect on Chl-a concentration. The turbulence generated by winds, surface heat fluxes, evaporation, sea ice formation has homogenized in the oceanic mixed layer at some range of depths.

The comparison of MLD, BLT (Figure 14) with Chl-a concentration

for Mala, Nilam as well as Phailin shows that in the effect of high winds the cool nutrient-rich water came up and upwelling occurred in the affected area and phytoplankton bloom dominated along the region. (Hudhud is not included due to the unavailability of accurate data). The BLT almost vanishes or reduces too much lower values. MLD has a maximum variation in the case of Phailin (30 m approx.) while Nilam shows a bimodal distribution. Chl-a concentration follows a similar pattern in all cases with the little phase difference. The results indicate that breakup of ocean stratifications during the passage of the TCs due to mixing have enhanced the values of MLD and led to increase in productivity. In pre-monsoon cyclone the mixed layer is shallow as compare to post monsoon cyclone and the barrier layer is shallow before the pre-monsoon cyclone like Mala while the deep barrier layer occurred before the post monsoon cyclones Nilam and Phailin as shown in Figure 14 [49].

Upwelling as a response of stratification parameter

In this section we elaborate the quantitative changes in stratification parameters in the 3 experiments to depict the individual role of wind stress curl and net heat flux on ocean mixing which in turn affects the surface Chl-a concentrations. During the winter months heat loss from the surface of the BoB results in an increase in density of surface waters and the water column become convectively unstable and produces vertical mixing. Likewise, during summer month's heat gained in the ocean surface through the atmosphere makes the surface water less dense thereby increasing the stratification which results in the less mixing or no mixing. Stratification again breaks through the onset of cooling and convective mixing as winter comes. The stratification parameter (φ) designates the potential energy anomaly [50]. Φ quantifies the potential energy required per unit volume for complete mixing of the water column. For a fully mixed ocean, the value of Φ is reportedly zero while it increases with stratification.

In order to understand the role of WSC and net heat flux on stratification, (φ) was computed for all four cyclones and calculated along the latitudinal section crossing the track of the cyclone for all the three model experiments (*viz.* Exp 1: control run with WSC +NHF, Exp 2: WSC only and Exp 3: NHF only as discussed in Section 1). Here we compare the stratification differences of different experiments to know the effect of the stratification parameter of NHF and WSC. The first comparison is the Φ difference between control and winds [51]. The second one is the difference of Φ between control and NHF whereas the third one shows the difference of Φ with winds and NHF. The results shown here are for pre and during different TCs.

During Mala cyclone, the Φ difference for Exp 1 (control) and Exp 2 (WSC) is positive whereas Φ difference for Exp 1 (control) and Exp 3 (NHF) turns negative as TC intensifies (Figure 15). Therefore, the stratification potential of NHF is high which intensifies stratification and reduced mixing for a period of pre and during the cyclone [52]. This can be attributed to the fact that in the summer months, the NHF is positive reducing the mixing. Again, the difference of Φ between Exp 2 (WSC) and Exp 3 (NHF) is negative showing positive NHF which causes reduced mixing whereas intense WSC increase mixing. But the increment in Chl-a is due to strong winds. Winds are strong enough to break the stratification initiated by NHF because Mala is an extremely severe cyclone witnessing very high winds.

For Nilam cyclone, the Φ difference for Exp 1 (control) and Exp 2 (WSC) is positive for both winds and NHF (Figure 16). Winds are not very strong during the Nilam cyclone because it is designated as a Tropical Storm. Positive difference of Φ for Exp 1 (control) and Exp 3(NHF) also suggest less mixing.
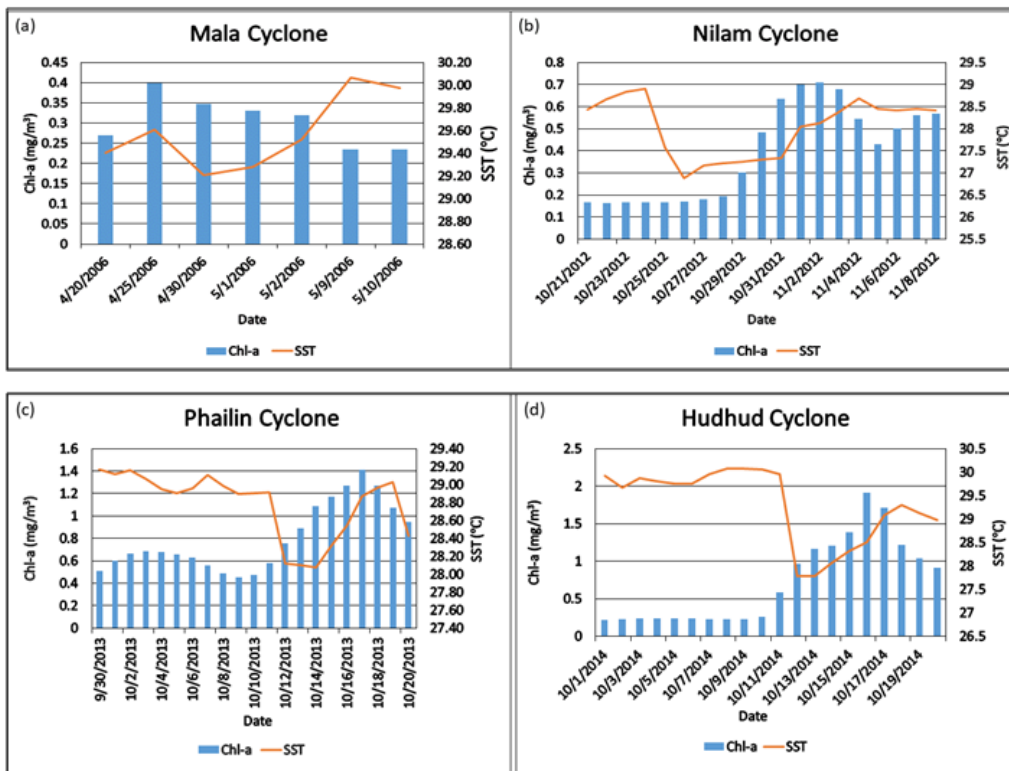
Figure 13: Comparison of Sea Surface Temperature (SST) with Chl-a concentration for (A) Mala (B) Nilam (C) Phailin (D) Hudhud. Note: Chl-a (▬); SST (▬).
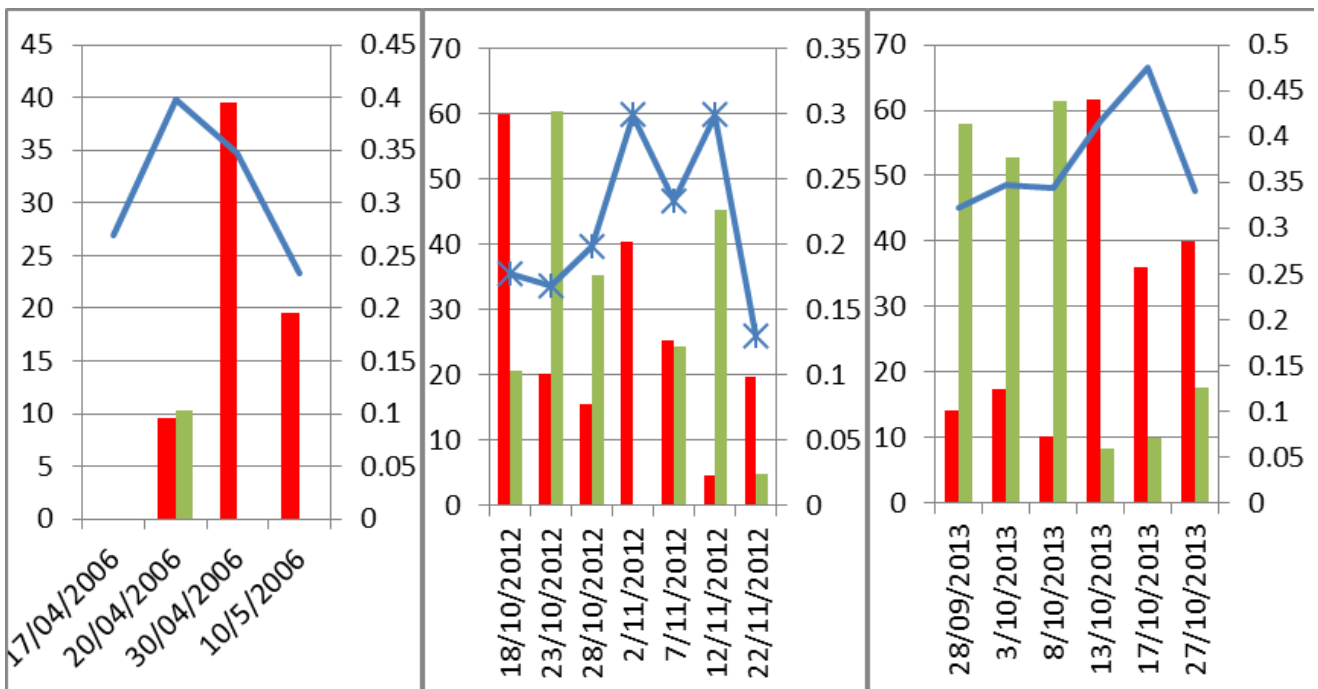

Figure 14: Comparison of wind-induced variations of MLD, BLT with Chl-a concentration during different stages of (a) Mala, (b) Nilam, and (c) Phailin. Note: MLD (▬); BLT (▬); Chlorophyll (▬).
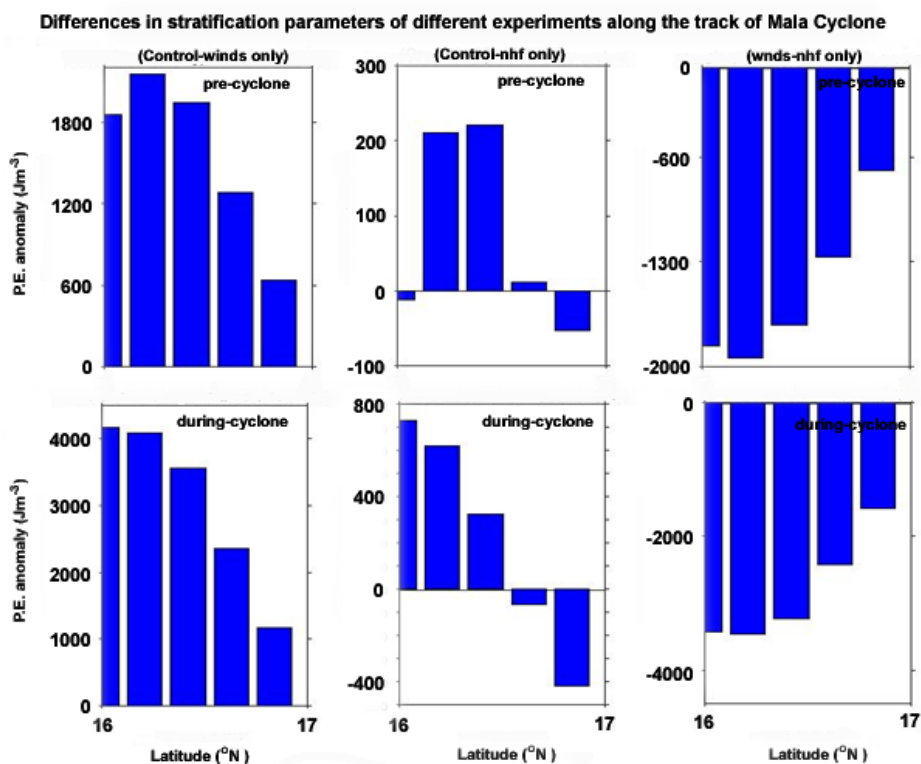
Figure 15: Stratification parameter for Mala cyclone for all three experiments for pre and during the cyclone.
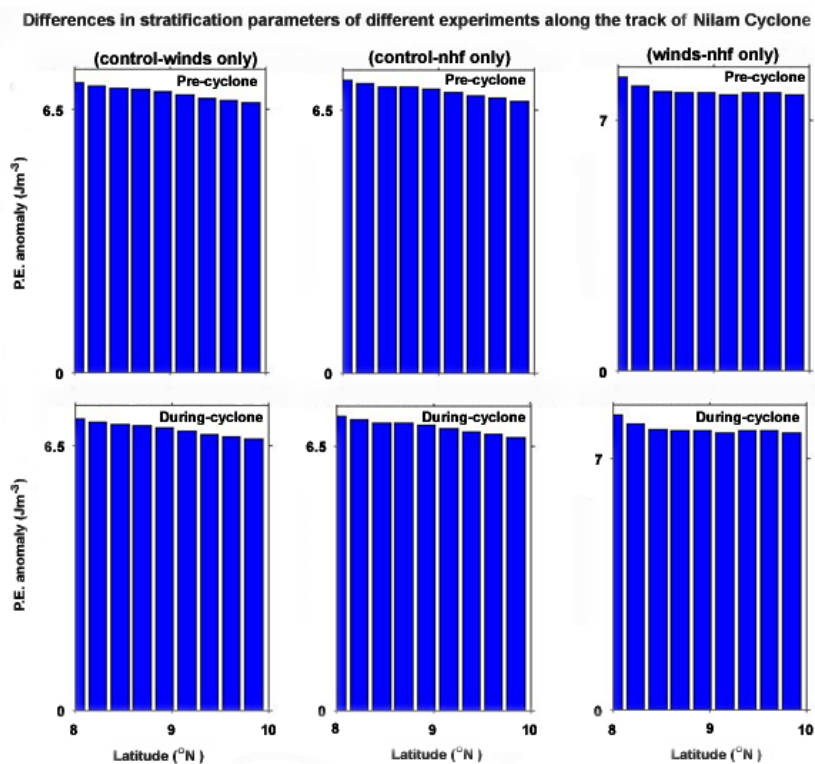

Figure 16: Stratification parameter for Nilam cyclone for all three experiments for pre and during the cyclone.

In case of Phailin, the stratification difference of Φ for Exp 1 (control) and Exp 2 (WSC) is negative as also the difference of Φ for Exp 1 (control) and Exp 3 (NHF) (Figure 17). This implies, the value of Φ is mostly higher for Exp 2 and the Exp 3. During the cyclonic event, Φ is positive (Exp.1) along 15˚N which indicates that Φ is positive for winds and no mixing occurred at this latitude due to winds. However, the difference of Φ for Exp 2 (WSC) and Exp 3 (NHF) is positive which implies higher stratification in WSC. Hence the results show the NHF induced mixing is more prominent as compared to wind-induced mixing during the Phailin cyclone. Generally, the oceanic NHF is also negative during winter which is a suitable condition for mixing.

Likewise, in the Hudhud cyclone, stratification difference of Φ for Exp 1 (control) and Exp 2 (WSC) shows a high stratification for WSC experiment (Figure 18). However, difference of Φ for Exp 1 (control) and Exp 3 (NHF) show a positive difference at initial phase which later turns negative. Therefore, initial stratification is higher in NHF experiment which gradually becomes lower than control experiment. This suggests that NHF causes higher mixing in the upper layer as TC

intensifies. Likewise, stratification difference of Φ for Exp 2 (WSC) and Exp 3 (NHF) shows that the Φ value of wind is high hence winds play less role in mixing as compare to the NHF.

From the above results, it is seen that during pre-monsoon cyclone Mala, extremely severe cyclone induced NHF is positive and oceanic NHF is also positive hence enhances stratification but winds are very strong during the cyclone period and which can break the stratification and produces upwelling of cold nutrient-rich water from the lower layers.

For post-monsoon cyclones like Nilam, the effect of WSC and NHF are almost similar. The cyclone Nilam is at a Tropical Storm stage and increased surface Chl-a during the cyclone has resulted in upwelling induced by winds and NHF [53]. The cyclones Phailin and Hudhud are extremely severe cyclonic events, hence winds and net heat flux is able to break the stratification and produced upwelling in both the cases (Table 3). However, the negative NHF is observed to play a more important role in mixing in these two cyclones as it generates heat loss from the ocean surface during winter months.
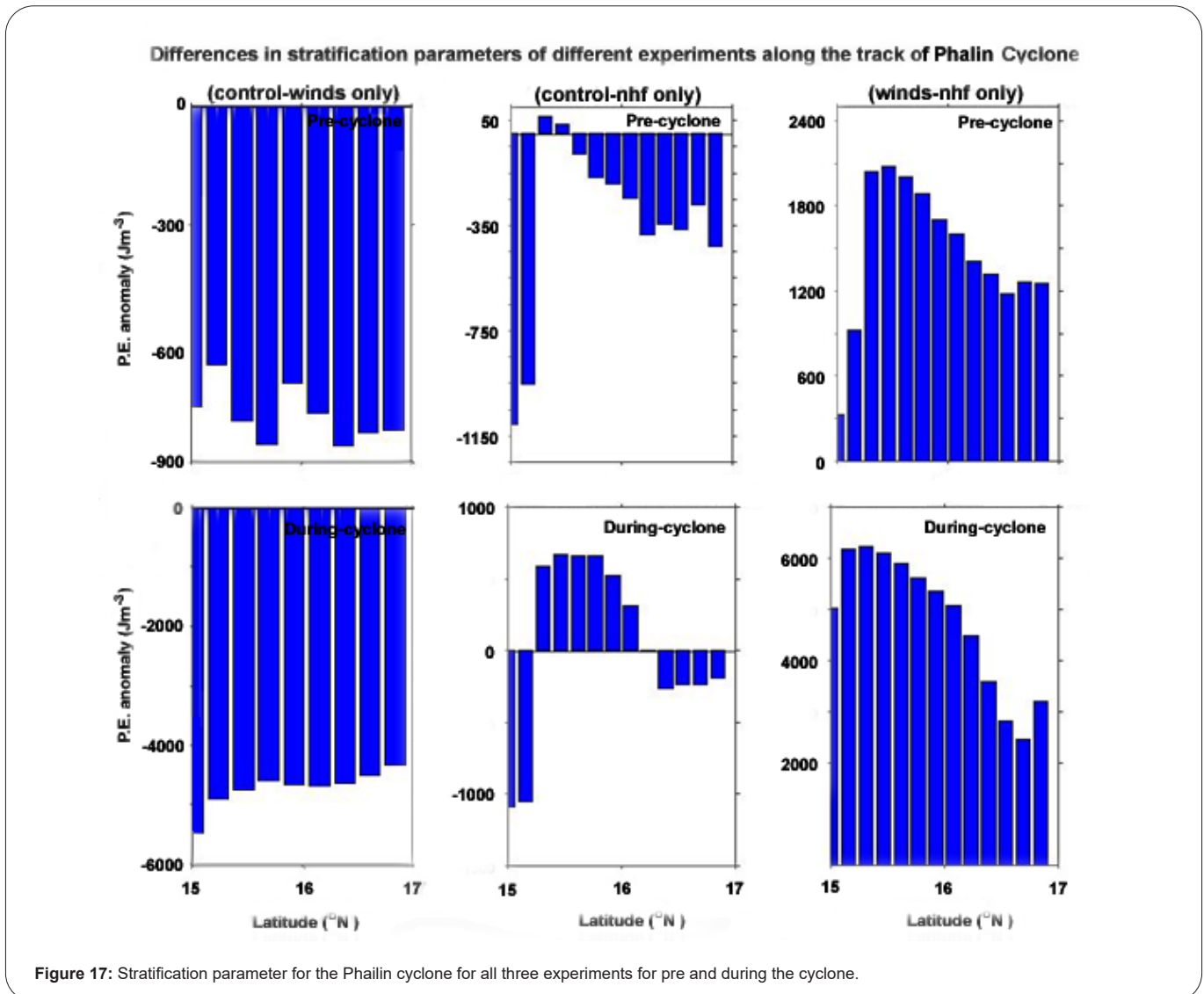

Figure 17: Stratification parameter for the Phailin cyclone for all three experiments for pre and during the cyclone.
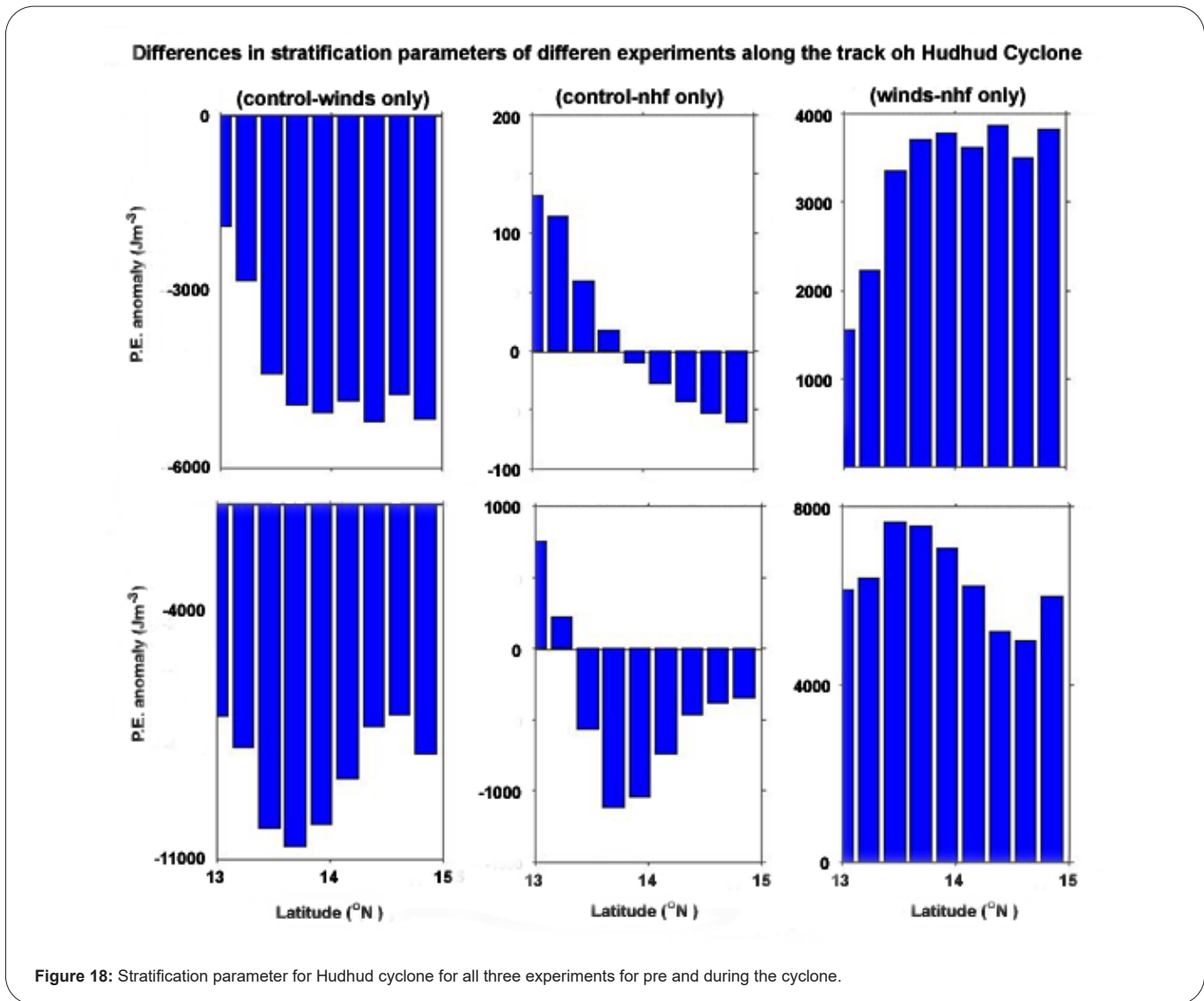
Figure 18: Stratification parameter for Hudhud cyclone for all three experiments for pre and during the cyclone.

Table 3: Variation of hydrographic features with Chl-a for various cyclones at their dissipation stage.

Cyclone Name	Category type	WSC (N/m²)	MLD (m)	BLT (m)	Chl-a (mg/m³)	SST (°C)
Mala	Extremely Severe Cyclonic Storm	-2.81 × 10-8	39.5	0	0.35	29.2
Nilam	Cyclonic Storm	1.1 × 10-8	40.4	0	0.3	28.7
Phailin	Extremely Severe Cyclonic Storm	2.4 × 10-8	61.7	8	0.52	28.5
Hudhud	Extremely Severe Cyclonic Storm	-5.5 × 10-9	62.3	0	0.59	29.1

Conclusion

The current study to understand the role of the physical mechanisms during Tropical Cyclone (TC) passage in different seasons that leads to the increase in the surface Chl-a concentration shows that TC-induced mixing (upwelling) and SST variation due to the combined effect of WSC and NHF has a prominent role on the variability of Chl-a concentration.

MLD increases during and after the passage of the cyclone. The

increase in MLD is less during Mala and Nilam which is up to 40 m while it increases up to 50 to 60 m for Phailin and Hudhud cyclones. The SSTs decreases from 1˚C to 2˚C during the passage of the different intense cyclones. The different model sensitivity experiments suggest that wind stress and net surface heat flux forcing promotes mixing the leading to increase in surface Chl-a concentrations during and after the cyclone passage. The model simulation with daily net heat as well as wind stress forcing can capture the increment in Chl-concentrations. The higher concentration in Chl-a in the model simulation may be

---

attributed to the model initial conditions derived from climatological spin up. In a sepertae research by Sreenivas the study of various oceanic processes on the life cycle of the cyclone 'Jal' have been done. They showed that influx of fresh water from precipitation/river runoff increased the density stratification. The resulted mixed layer is shallow and determined by the salinity stratification and isothermal layer is deeper resulted barrier layer. Barrier layer acts as a barrier to momentum mixing and keeps the influence of atmospheric heat and momentum forcing predominantly in the surface mixed layer inhibit mixing from cool thermocline water to surface mixed layer water. Another study for cold core cyclones in Gulf of Mexico done by Walker showed that thermocline upwelled from depths of 53 to 62 m within the areas of maximum SST change. Chl-a concentration response to the typhoon was studied by Liu and they concluded that the Net Heat Flux (air-sea heat exchange) played a major role in controlling the upper ocean physical processes through cooling the SST and indirectly increased the surface Chl-a until two weeks after the typhoon.

We conclude that the incorporation of daily wind stress and net heat flux can significantly improve the prediction of cyclone-induced Chl-a enrichments. This study therefore, provides the role of TC induced stratification changes on Chl-a concentration changes which can have significant influence on ocean's productivity. A long-term assessment of these upper ocean changes under varying intensity TCs in future climate can helps use to understand future changes of Chl-a concentration.

Acknowledgement

References

1. NEmanuel KA (1986) An air-sea interaction theory for tropical cyclones. Part I: Steady-state maintenance. J Atmos Sci 43(6):585-605.

2. Rao AD, Dash S, Babu SV, Jain I (2007) Numerical modeling of cyclone's impact on the ocean: A case study of the Orissa super cyclone. J Coast Res 23(5):1245-50.

3. Bates NR, Knap AH, Michaels AF (1998) Contribution of hurricanes to local and global estimates of air–sea exchange of CO_2. Nature 395(6697):58-61.

4. Holland G, Bruyère CL (2014) Recent intense hurricane response to global climate change. Clim. Dyn. 42:617-27.

5. Knutson T, Camargo SJ, Chan JC, Emanuel K, Ho CH, et al. (2020) Tropical cyclones and climate change assessment: Part II: Projected response to anthropogenic warming. Bull Am Meteorol Soc 101(3):E303-22.

6. Webster PJ, Holland GJ, Curry JA, Chang HR (2005) Changes in tropical cyclone number, duration, and intensity in a warming environment. Science 309(5742):1844-6.

7. Lin I, Liu WT, Wu CC, Wong GT, Hu C, et al., (2003) New evidence for enhanced ocean primary production triggered by tropical cyclone. Geophys Res Lett 30(13).

8. Mei W, Xie SP, Primeau F, McWilliams JC, Pasquero C, et al., (2015) Northwestern Pacific typhoon intensity controlled by changes in ocean temperatures. Sci Adv 1(4):e1500014.

9. Liu F, Tang S (2018) Influence of the interaction between typhoons and oceanic mesoscale eddies on phytoplankton blooms. J Geophys Res Oceans 123(4):2785-94.

10. Shi W, Wang M (2007) Observations of a hurricane Katrina-induced phytoplankton bloom in the Gulf of Mexico. Geophys Res Lett 34(11).

11. Parker CL, Lynch AH, Spera SA, Spangler KR (2017) The Relationship between tropical cyclone activity, nutrient loading, and algal blooms over the Great Barrier Reef. Biogeosci Discuss 6:1-35.

12. Singh OP, Khan TM, Rahman MS (2001) Has the frequency of intense tropical cyclones increased in the north Indian Ocean?. Curr Sci 25:575-80.

13. Balaguru K, Taraphdar S, Leung LR, Foltz GR (2014) Increase in the intensity of postmonsoon Bay of Bengal tropical cyclones. Geophys Res Lett 41(10):3594-60.

14. Balaji, M., Chakraborty, A., and Mandal, M. (2018) Changes in tropical cyclone activity in the north Indian Ocean during the satellite era. Int J Climatol 38(6): 2819–2837.

15. Alam M, Hossain A, S.Shafee (2003) Frequency of Bay of Bengal cyclonic storms and depressions crossing different coastal zones. Int J Climatol 23(9):1119–1125.

16. Mahala BK, Nayak BK, Mohanty PK (2015) Impacts of ENSO and IOD on tropical cyclone activity in the Bay of Bengal. Nat Hazards 75:1105-25.

17. Gadgil S, Gadgil S (2006) The Indian monsoon, GDP and agriculture. Econ Polit Wkly 25:4887-95.

18. Jacob SD, Shay LK, Mariano AJ, Black PG (2000) The 3D oceanic mixed layer response to Hurricane Gilbert. J Phys Oceanogr 30(6):1407-29.

19. Price JF (1981) Upper ocean response to a hurricane. J Phys Oceanogr 11(2):153-75.

20. Sanford TB, Price JF, Girton JB (2011) Upper-ocean response to Hurricane Frances (2004) observed by profiling EM-APEX floats. J Phys Oceanogr 41(6):1041-56

21. Shay LK, Black PG, Mariano AJ, Hawkins JD, Elsberry RL, et al.,(1992) Upper ocean response to Hurricane Gilbert. J Geophys Res Oceans 97(C12):20227-48.

22. O'Brien JJ, Reid RO (1967) The non-linear response of a two-layer, baroclinic ocean to a stationary, axially-symmetric hurricane: Part I. Upwelling induced by momentum transfer. J Atmos Sci 24(2):197-207.

23. Murty VS, Rao DP, Sastry JS (1983) The lowering of sea surface temperature in East Central Arabian Sea associated with a cyclone. Mahasagar- Bulletin of National Institute of Oceanography 16 (1): 67-71.

24. Premkumar K, Ravichandran M, Kalsi SR, Sengupta D, Gadgil S(2000) First results from a new observational system over the Indian seas. Curr. Sci 78(3):323-30.

25. Vissa NK, Satyanarayana AN, Prasad Kumar B (2013) Response of oceanic cyclogenesis metrics for NARGIS cyclone: A case study. Atmos Sci Lett 14(1):7-13.

26. Vinayachandran PN, Mathew S (2003) Phytoplankton bloom in the Bay of Bengal during the northeast monsoon and its intensification by cyclones. Geophys Res Lett 30(11)

27. Sarangi Rk (2011) Impact of cyclones on Bay of Bengal chlorophyll variability using remote sensing satellites, Indian J Mar Sci 40(6): 794-801

28. Byju P, Kumar SP [2011] Physical and biological response of the Arabian Sea to tropical cyclone Phyan and its implications. Mar Environ Res 71(5):325-30.

29. Subrahmanyam B, Rao KH, Srinivasa Rao N, Murty VS, Sharp RJ et al., (2002) Influence of a tropical cyclone on chlorophyll-a concentration in the Arabian Sea. Geophys Res Lett 29(22):22-1.

30. Sarangi RK (2016) Remote sensing observations of ocean surface chlorophyll and temperature with the impact of cyclones and depressions over the Bay of Bengal Water, Mar. Geod 39 (1):53–76.

31. Chacko, N. and Zimik, L (2018). Effect of cyclone Thane in the Bay of Bengal explored using moored buoy observations and multi-platform satellite data. J Indian Soc Remote Sens 46:821-8.

32. Krishna, K. M. (2013). Cyclone persuade on chlorophyll-A enrichment in the Bay of Bengal. Geosci 2 (4): 1-3.

33. Neetu S, Lengaigne M, Vincent EM, Vialard J, Madec G, et al.,(2012) Influence of upper-ocean stratification on tropical cyclone-induced surface cooling in the Bay of Bengal. J Geophys Res Oceans 117(C12020)

34. Shchepetkin AF, McWilliams (2005) The regional oceanic modeling system (ROMS): a split-explicit, free-surface, topography-following-coordinate oceanic model. Ocean Model 9(4):347-404.

35. Large WG, McWilliams JC, Doney SC (1994) Oceanic vertical mixing: A review and a model with a nonlocal boundary layer parameterization. Rev Geophys 32(4):363-403.

36. Fasham MJ, Ducklow HW, McKelvie SM (1990). A nitrogen-based model of plankton dynamics in the oceanic mixed layer. J. Mar. Res. 48(3):591-639.

37. Evans GT, Parslow JS(1985) A model of annual plankton cycles. Biological oceanography 3(3):327-47.

38. Mukhopadhyay SK, Biswas HD, De TK, Jana TK (2006) Fluxes of nutrients from the tropical River Hooghly at the land–ocean boundary of Sundarbans, NE Coast of Bay of Bengal, India. J Mar Syst 62(1-2):9-21.

39. Balaguru K, Taraphdar S, Leung LR, Foltz GR (2014) Increase in the intensity of postmonsoon Bay of Bengal tropical cyclones. Geophys Res Lett 41(10):3594-60.

40. Smitha A, Rao KH, Sengupta D (2006) Effect of May 2003 tropical cyclone on physical and biological processes in the Bay of Bengal. Int J Remote Sens 27(23):5301-14.

41. Goni G, Kamholz S, Garzoli S, Olson D (1996). Dynamics of the Brazil-Malvinas Confluence based on inverted echo sounders and altimetry. J Geophys Res Oceans 101(C7):16273-89.

42. Willis JK, Roemmich D, Cornuelle B (2004) Interannual variability in upper ocean heat content, temperature, and thermosteric expansion on global scales. 109(C12)

43. Ali MM, Singh N, Kumar MS, Zheng Y, Bourassa M, et al. (2018) Dominant modes of upper ocean heat content in the north Indian Ocean. climate 6(3):71.

44. Sreenivas P, Gnanaseelan C, Prasad KV (2012) Influence of El Niño and Indian Ocean Dipole on sea level variability in the Bay of Bengal. Glob Planet Change 80:215-25.

45. McPhaden MJ, Foltz GR, Lee T, Murty VS, Ravichandran M et al., (2009) Ocean-atmosphere interactions during cyclone nargis. EOS, Transactions American Geophysical Union 90(7):53-4.

46. Price JF (1981) Upper ocean response to a hurricane. J Phys Oceanogr 11(2):153-75.

47. Pudov VD (1992)The ocean response to the cyclone's influence and its possible role in their track formation. InICSU/WMO international symposium on tropical cyclone disasters 367-376

48. DeMaria M, Kaplan J, (1994) A Statistical Hurricane Prediction Scheme (SHIPS) for the Atlantic basin, Weather Forecast 9: 209–220.

49. Sengupta D, Goddalehundi BR, Anitha DS (2008) Cyclone-induced mixing does not cool SST in the post-monsoon north Bay of Bengal. Atmos Sci Lett 9(1):1-6.]

50. Simpson JH, Tett PB, Argote-Espinoza ML, Edwards A, Jones KJ, et al., (1982) Mixing and phytoplankton growth around an island in a stratified sea. Cont. Shelf Res 1(1):15-31.

51. Sreenivas P, Gnanaseelan C (2013) Impact of oceanic processes on the life cycle of severe cyclonic storm "Jal". IEEE Geosci Remote Sens Lett 11(2):519-23.

52. Walker ND, Leben RR, Balasubramanian S (2005) Hurricane-forced upwelling and chlorophyll a enhancement within cold-core cyclones in the Gulf of Mexico. Geophys Res Lett 28;32(18).

53. Liu Y, Tang D, Evgeny M (2019) Chlorophyll concentration response to the typhoon wind-pump induced upper ocean processes considering air–sea heat exchange. Remote Sens 11(15):1825.